# Supporting Information

# High-Temperature Superconductivity in a Th-H System under Pressure Conditions

*Alexander G. Kvashnin,* [1,2,*] *Dmitrii V. Semenok,* [1,2] *Ivan A. Kruglov,* [2,3] *Izabela A. Wrona,* [4] *Artem R. Oganov,* [1,2,3,5*]

[1] Skolkovo Institute of Science and Technology, Skolkovo Innovation Center 143026, 3 Nobel Street, Moscow, Russia

[2] Moscow Institute of Physics and Technology, 141700, 9 Institutsky lane, Dolgoprudny, Russia

[3] Dukhov Research Institute of Automatics (VNIIA), Moscow 127055, Russia

[4] Institute of Physics, Jan Dlugosz University in Czestochowa, Ave. Armii Krajowej 13/15, 42-200 Czestochowa, Poland

[5] International Center for Materials Discovery, Northwestern Polytechnical University, Xi'an, 710072, China

**Corresponding Authors**

*A.G. Kvashnin, E-mail: A.Kvashnin@skoltech.ru

*A.R. Oganov, E-mail: A.Oganov@skoltech.ru

## Crystal structures of Th-H phases

Table S1. Crystal structures of predicted Th-H phases. Volume, density and lattice parameters and coordinates are given for the lowest pressure value within the stability range.

| *Phase* | *Pressure range, GPa* | *Volume per unit, Å³* | *ρ, g/cm³* | *Lattice parameters* | *Coordinates* | | | |
|---|---|---|---|---|---|---|---|---|
| $C2/m$-$ThH_2$ | 0-15 | 39.78 | 9.55 | a = 4.91 Å, b = 5.95 Å, c = 3.68 Å, β = 132.14° | Th | 0.000 | 0.000 | 0.500 |
| | | | | | H | 0.000 | -0.249 | 0.000 |
| $R\bar{3}m$-$ThH_3$ | 90-100 | 24.47 | 15.35 | a = b = 2.96 Å, c = 9.67 Å, γ = 120° | Th | 0.000 | 0.000 | 0.500 |
| | | | | | H | 0.000 | 0.000 | 0.000 |
| | | | | | H | 0.000 | 0.000 | 0.289 |
| $Immm$-$Th_3H_{10}$ | 10-85 | 110.16 | 10.29 | a = 12.98 Å, b = 4.11 Å, c = 4.27 Å | Th | -0.331 | 0.000 | 0.000 |
| | | | | | Th | 0.000 | 0.000 | 0.000 |
| | | | | | H | 0.154 | 0.000 | -0.242 |
| | | | | | H | 0.083 | 0.500 | 0.000 |
| | | | | | H | -0.232 | 0.500 | 0.000 |
| | | | | | H | 0.000 | -0.254 | 0.500 |
| $Pnma$-$ThH_4$ | 5-10 | 44.68 | 8.77 | a = 6.65 Å, b = 4.23 Å, c = 6.35 Å | Th | 0.263 | 0.250 | 0.094 |
| | | | | | H | 0.436 | -0.018 | -0.156 |
| | | | | | H | -0.302 | 0.250 | -0.242 |
| | | | | | H | 0.391 | 0.250 | 0.443 |
| $P321$-$ThH_4$ | 15-85 | 38.34 | 10.83 | a = b = 5.96 Å, c = 3.73 Å, γ = 120° | Th | 0.000 | 0.000 | 0.500 |
| | | | | | Th | 0.333 | 0.667 | 0.210 |
| | | | | | H | 0.355 | 0.000 | 0.500 |
| | | | | | H | 0.239 | 0.000 | 0.000 |
| | | | | | H | -0.086 | -0.420 | 0.270 |
| $I4/mmm$-$ThH_4$ | 85-300 | 27.11 | 14.46 | a = b = 3.00 Å, c = 6.02 Å, | Th | 0.000 | 0.000 | 0.000 |
| | | | | | H | 0.000 | 0.500 | 0.250 |
| | | | | | H | 0.000 | 0.000 | 0.364 |
| $Cmc2_1$-$ThH_6$ | 25-90 | 41.64 | 9.49 | a = 3.99 Å, b = 6.55 Å, c = 6.38 Å | Th | 0.000 | -0.346 | -0.347 |
| | | | | | H | 0.000 | -0.086 | 0.393 |
| | | | | | H | 0.000 | 0.002 | 0.115 |
| | | | | | H | 0.000 | -0.320 | 0.029 |
| | | | | | H | 0.260 | 0.093 | 0.347 |
| | | | | | H | 0.000 | 0.201 | -0.164 |
| $P2_1/c$-$ThH_7$ | 85-115 | 33.94 | 11.69 | a = 6.09 Å, b = 3.93 Å, c = 5.78 Å, β = 78.23° | Th | -0.204 | 0.000 | 0.263 |
| | | | | | H | 0.088 | 0.224 | 0.088 |
| | | | | | H | 0.000 | -0.257 | 0.500 |
| | | | | | H | 0.303 | 0.000 | 0.105 |
| | | | | | H | 0.433 | 0.000 | 0.147 |
| | | | | | H | -0.425 | 0.000 | -0.387 |
| | | | | | H | -0.130 | 0.000 | -0.373 |
| $I\bar{4}3d$-$Th_4H_{15}$ | 0-10 | 188.75 | 8.29 | a = b = c = 9.04 Å | Th | 0.292 | 0.292 | 0.292 |
| | | | | | H | -0.126 | 0.222 | 0.094 |
| | | | | | H | 0.875 | 0.000 | 0.250 |
| $Fm\bar{3}m$-$ThH_{10}$ | 100-300 | 38.48 | 10.45 | a = b = c = 5.22 Å | Th | 0.000 | 0.000 | 0.000 |
| | | | | | H | 0.250 | 0.250 | 0.250 |
| | | | | | H | -0.377 | -0.377 | -0.377 |

It can be seen from Fig. S1a that $R\bar{3}m$-$ThH_3$ phase has a layered structure, where Th atoms occupy (0,0,0) positions and hydrogen atoms are in between thorium layers. Coordination number of thorium in this structure equals to 14 and distance between Th and H (d(Th-H)) equals

to 2.1 Å at 90 GPa (see Fig. S1a). The shortest distance between hydrogen atoms in the layer is 1.8 Å, so they do not form a chemical bond in $R\bar{3}m$-$ThH_3$. Layered structure of $R\bar{3}m$-$ThH_3$ phase directly impacts on the electronic properties. Flat bands are seen in the Γ→A, L→M and K→H directions, which are perpendicular to the layers. The electronic density at Fermi level mainly comes from thorium atoms (red bands in Fig. S1a). The crystal structure of *Immm*-$Th_3H_{10}$ phase contains 12-coordinate thorium atoms in the bcc arrangement (with Th-H distance of 2.28 Å at 10 GPa) and hydrogen atoms laying along the [1,0,0], [0,1,0] and [0,0,1] planes (see Fig. S1b). $ThH_4$ phase has orthorhombic lattice with thorium atoms in (0,0,0) positions. Each thorium atom is surrounded by 12 hydrogen atoms (see Fig. S1c). The H-H distance varies from 1.57 to 1.65 Å.

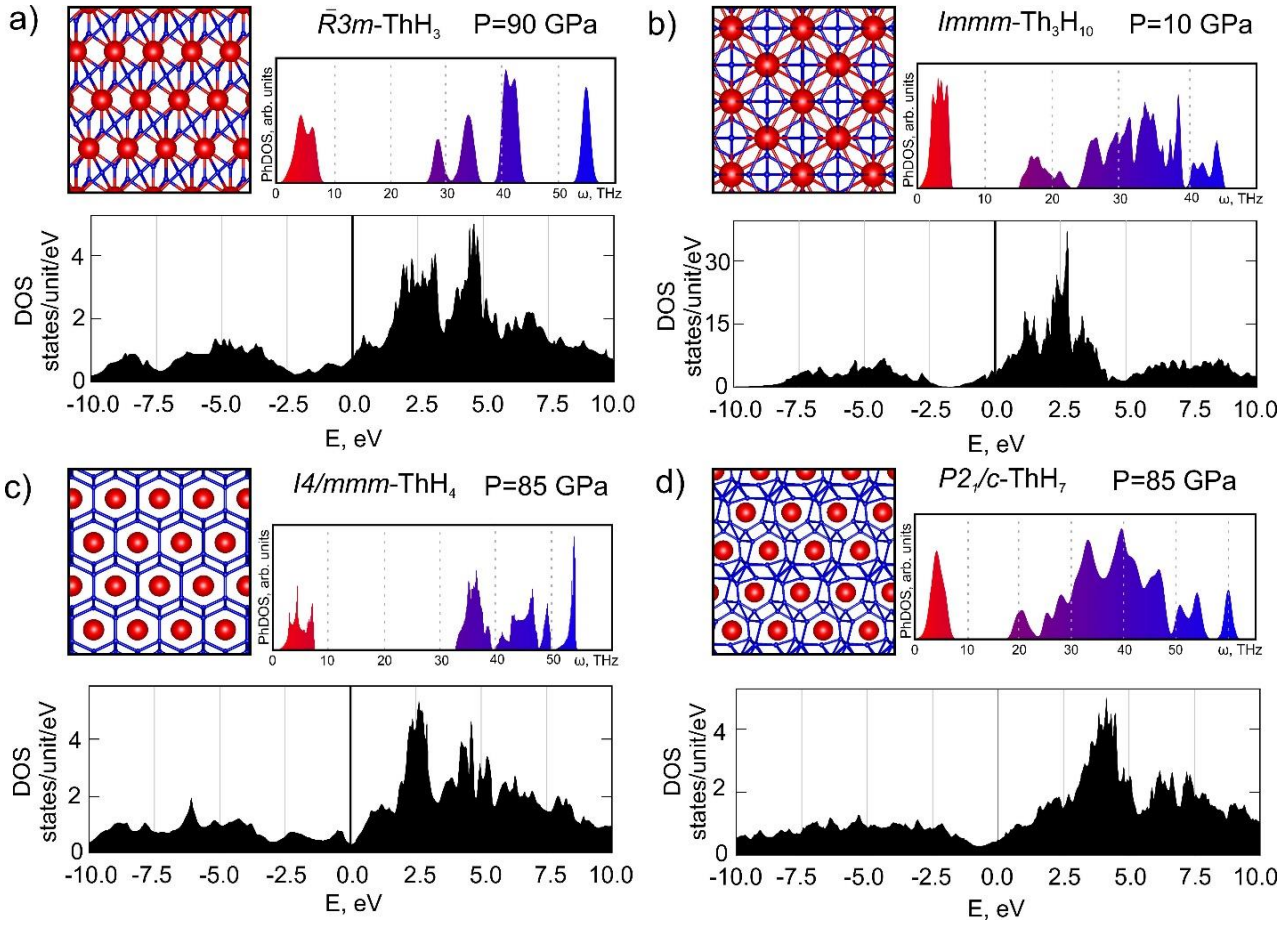


Fig. S1. Crystal structure, phonon density of states, electronic band structure and density of states for predicted a) $R\bar{3}m$-$ThH_3$, b) *Immm*-$Th_3H_{10}$ c) $I4/mmm$-$ThH_4$ and d) $P2_1/c$-$ThH_7$.

## Equations for calculating $T_C$

Calculations were made using the Eliashberg equations which take the following form (on the imaginary axis)[1]:

$$\phi_n = \frac{\pi}{\beta} \sum_{m=-M}^{M} \frac{\lambda(i\omega_n - i\omega_m) - \mu^* \theta(\omega_c - |\omega_m|)}{\sqrt{\omega_m^2 Z_m^2 + \phi_m^2}} \phi_m \tag{S1}$$

$$Z_n = 1 + \frac{1}{\omega_n} \frac{\pi}{\beta} \sum_{m=-M}^{M} \frac{\lambda(i\omega_n - i\omega_m)}{\sqrt{\omega_m^2 Z_m^2 + \phi_m^2}} \omega_m Z_m \tag{S2}$$

where: $\phi_n$ – the order parameter function, $Z_n$ - the wave function renormalization factor, θ(x) - Heaviside function, $\omega_n = \pi \cdot k_B T \cdot (2n\text{-}1)$ - the $n$-th Matsubara frequency, $\beta = k_B T$, $\mu^*$ - Coulomb pseudopotential, $\omega_c$ - the cut-off energy ($\omega_c = 3\Omega_{max}$, $\Omega_{max}$ – maximum frequency in $\alpha^2 F(\omega)$). The electron-phonon pairing kernel:

$$\lambda(z) = 2 \int_0^{\Omega_{max}} \frac{\alpha^2 F(\Omega)}{\Omega^2 - z^2} \Omega \, d\Omega \tag{S3}$$

The Eliashberg equations have been solved for 2201 Matsubara frequencies, starting from $T_0$ = 10K (below this temperature, the solutions are not stable). The methods discussed in the papers[2–4] were used during the calculations.

The full form of the order parameter and the wave function renormalization factor on the real axis was obtained through analytical extension of the Eliashberg equations solutions from the imaginary axis, using the formula:

$$X(\omega) = \frac{p_1 + p_2\omega + ... + p_r\omega^{r-1}}{q_1 + q_2\omega + ... + q_r\omega^{r-1} + \omega^r} \tag{S4}$$

where $X \in \{\Delta; Z\}$, r = 50. The values of $p_j$ and $q_j$ parameters were selected in accordance with the principles presented at work[5]. The obtained results allow to calculate dimensionless parameter $R_C$ (relative jump of the specific heat), using the formula below:

$$R_C = \frac{C^S(T_C) - C^N(T_C)}{C^N(T_C)} \tag{S5}$$

Because of strong-coupling and retardation effects, parameter $R_C$ (3.21 for $ThH_{10}$ at 100 GPa) differs significantly from BCS theory prediction, in which the constant value is equal to 1.43[6].

Physically $Z_{m=1}$ determines approximate ratio of the renormalized electron mass ($m_e^*$) to the electron band mass ($m_e$). The wave function renormalization factor on the real axis (see Supporting Information) allows the precise calculation of the renormalized electron mass ($m_e^*$) using the formula $m_e^* = Re[Z(\omega = 0)] \cdot m_e$. The renormalized highest mass of the electron corresponds to the critical temperature, but the exact values are presented in the Table 2.

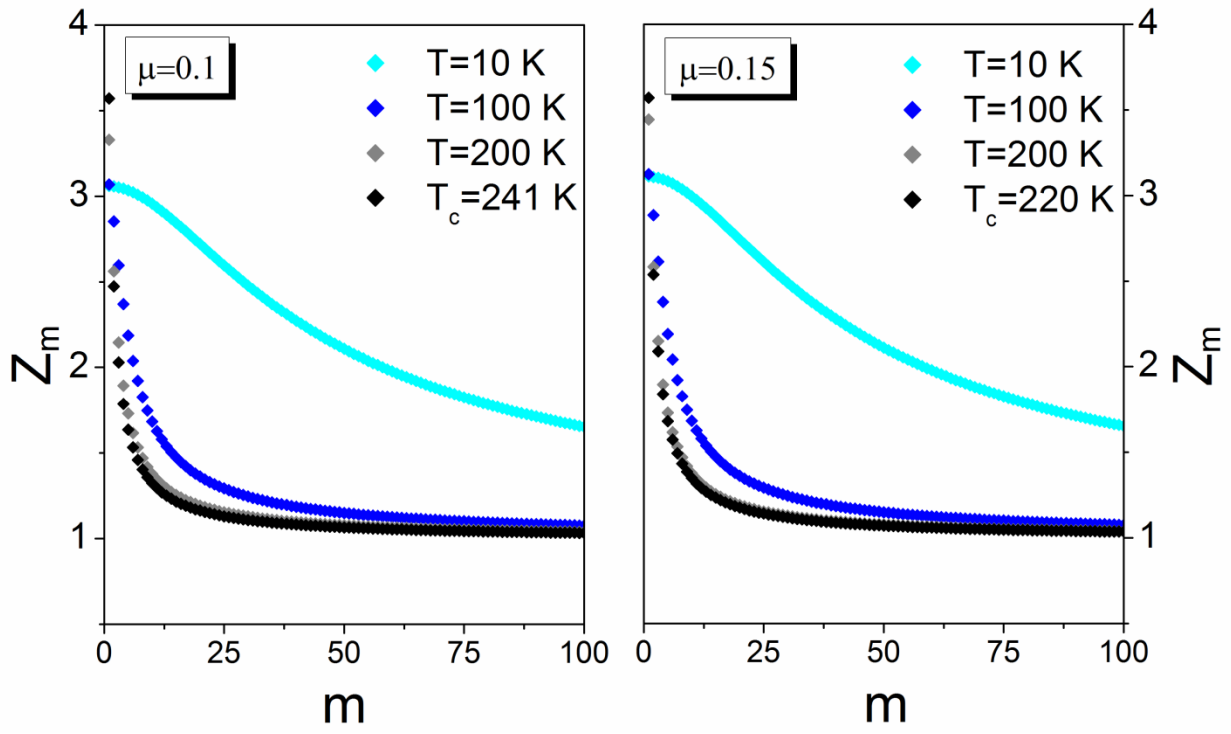


Fig. S2. The wave function renormalization factor on the imaginary axis for the selected values of temperature ($Fm\bar{3}m$-$ThH_{10}$ at 100 GPa, the first 100 values of m).

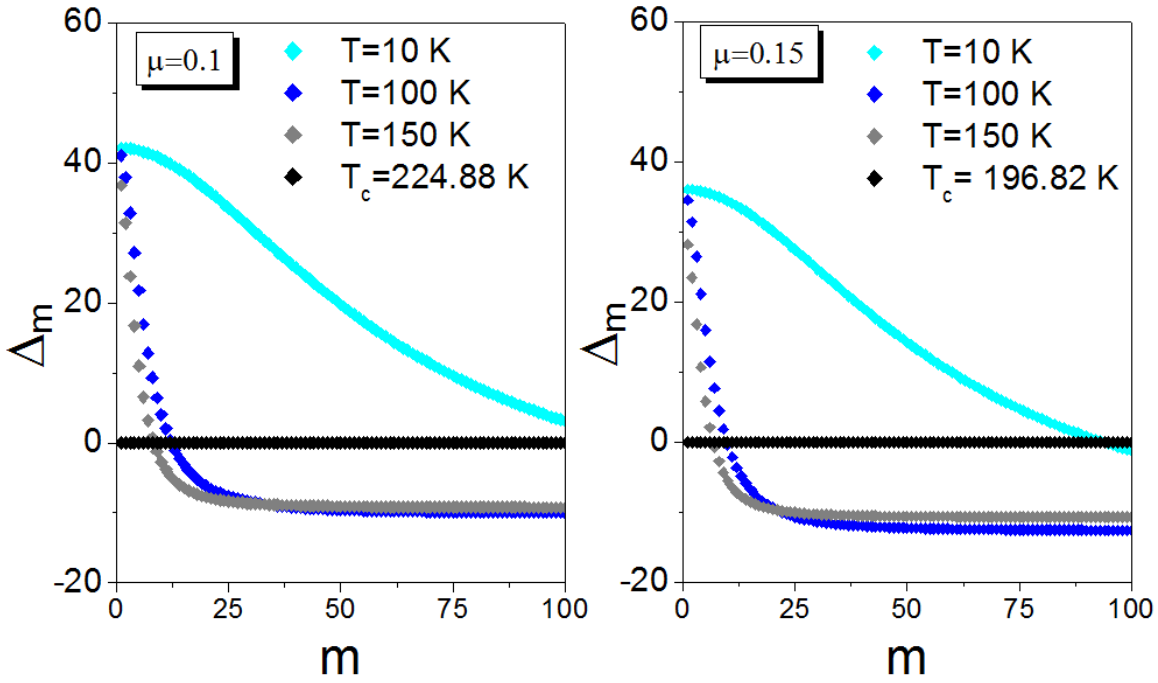


Fig. S3. The superconducting order parameter on the imaginary axis for the selected values of temperature ($Fm\bar{3}m$-$ThH_{10}$ at 200 GPa, the first 100 values of m).

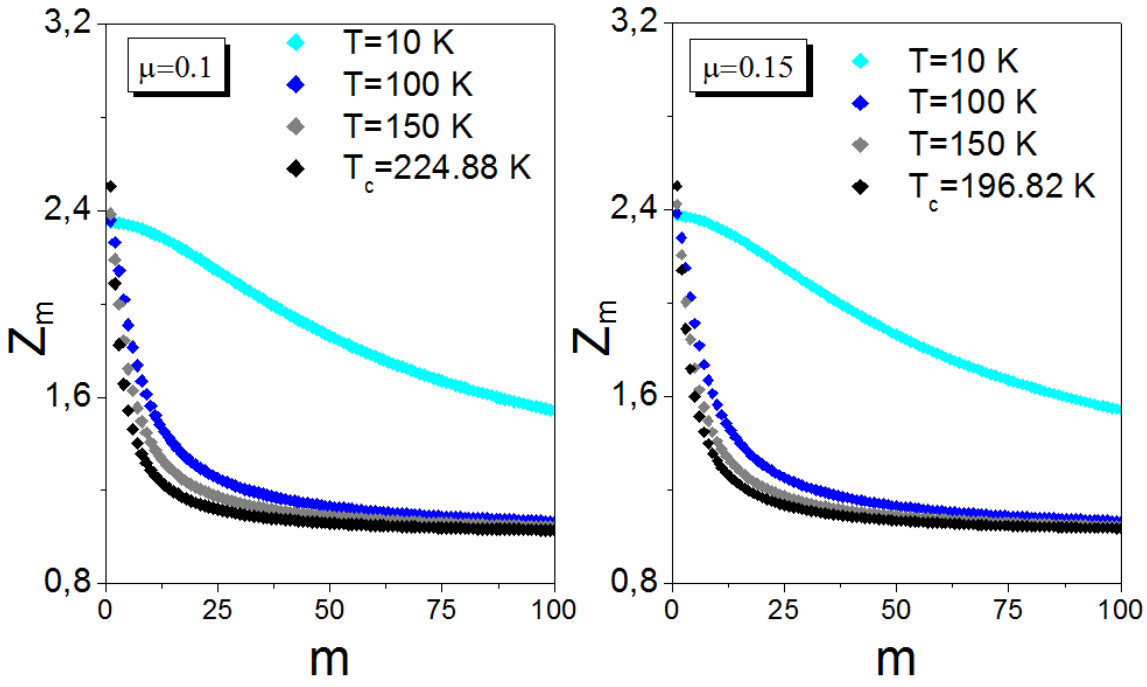


Fig. S4. The wave function renormalization factor on the imaginary axis for the selected values of temperature ($Fm\bar{3}m$-$ThH_{10}$ at 200 GPa, the first 100 values of m).

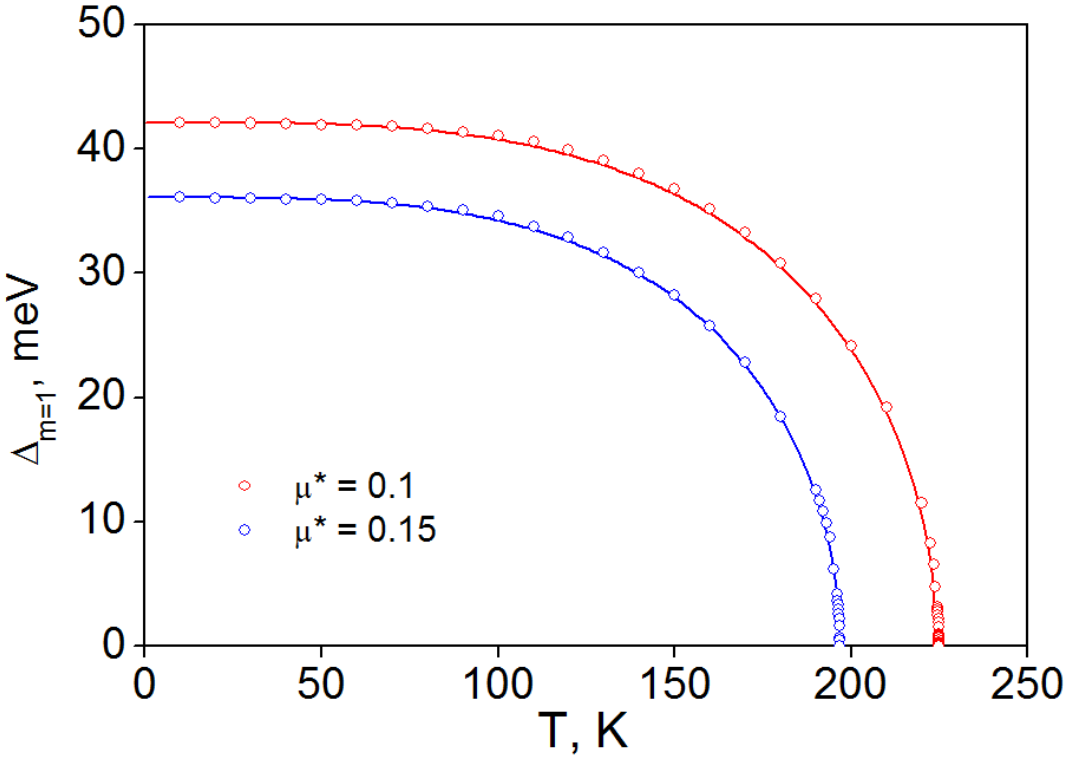


Fig. S5. The temperature dependence of the maximum value of the order parameter in $Fm\bar{3}m$-$ThH_{10}$ at 200 GPa. The lines are obtained by Eq. 8.

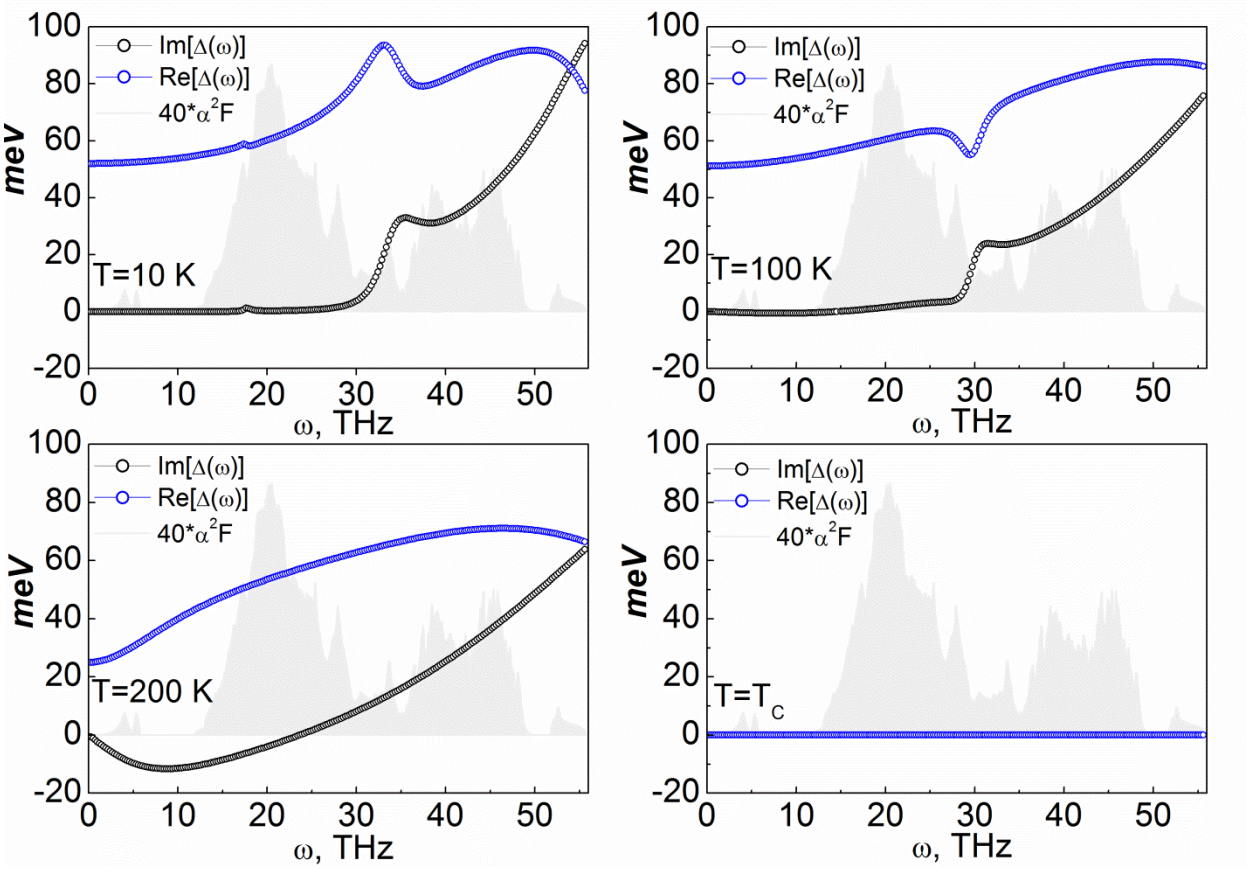


Fig. S6. The order parameter on the real axis in $Fm\bar{3}m$-$ThH_{10}$ at 100 GPa for the selected values of temperature ($\mu*$=0.1). In addition, the Eliashberg function (grey) was added as the background (multiplied by 40 for easier comparison).

Table S2. Parameters of superconductive state in several hydrides at optimal pressures and $\mu*$=0.1. For the cuprates and pnictides all values were obtained experimentally.

| Compound | SC gap, meV | $T_C$, K |
|---|---|---|
| $ThH_{10}$ | 52 | 241 |
| $LaH_{10}$[8] | 68 | 286 |
| $YH_{10}$[8] | 77 | 326 |
| $H_3S$[9] | 42.7 | 203 |
| $BiH_6$[10] | 18.1 | 100 |
| $PH_3$[11] | 14.5 | 81 |
| $YH_3$[12] | 8.4 | 45.9 |
| $H_3Se$[13] | 28.4 | 131 |
| $MgH_6$ [14] | 106.6 | 420 |
| $YBa_2Cu_3O_{7-y}$[15] | 34 | 92 |
| $NdBa_2Cu_3O_7$[16] | 30 | 95 |
| $Bi_2Sr_2Ca_2Cu_3O_{10+y}$[17] | 45 | 111 |
| $SmFeAsO_{0.9}F_{0.1}$[18] | 15 | 44 |
| $Ba_{0.6}K_{0.4}Fe_2As_2$[19] | 12 | 37 |

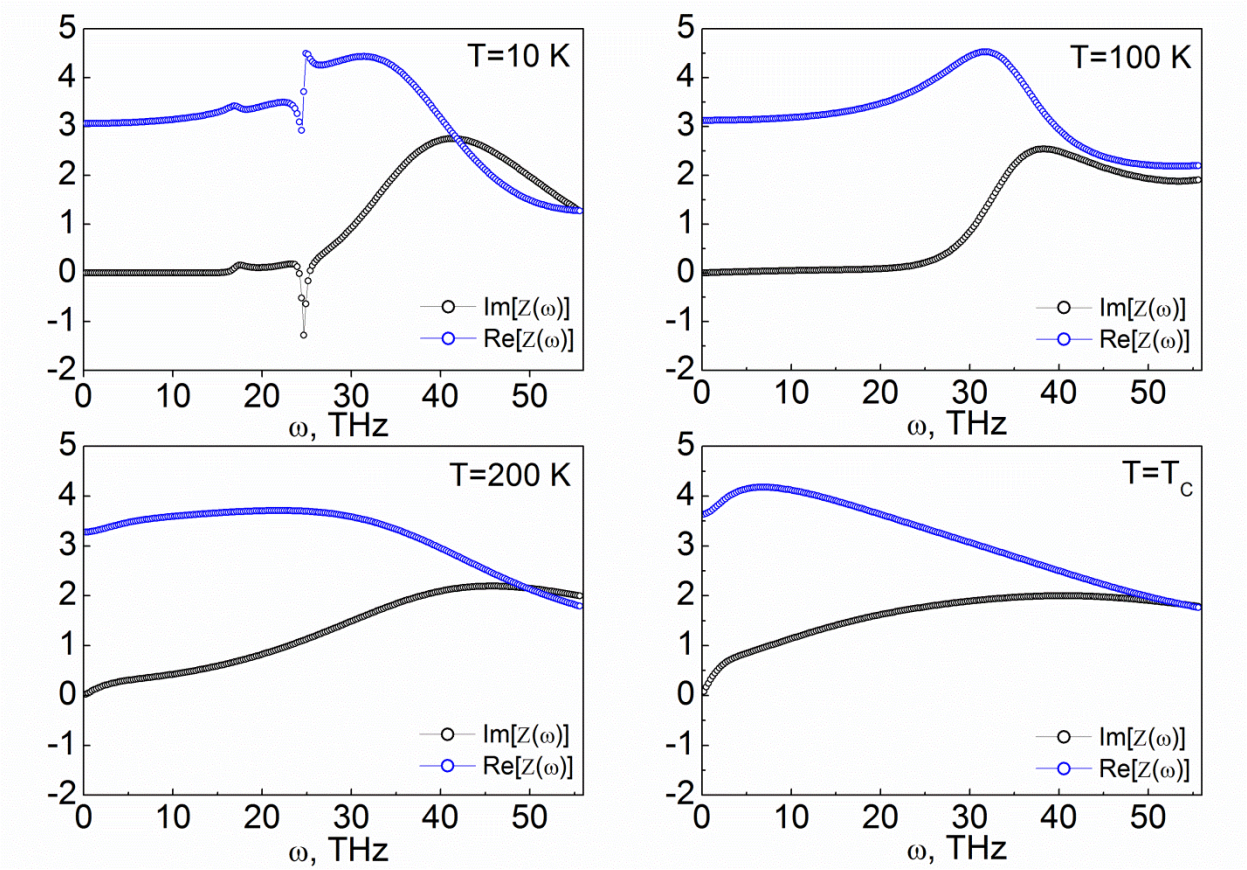


Fig. S7. The wave function renormalization factor in $Fm\bar{3}m$-$ThH_{10}$ at 100 GPa on the real axis for the selected values of temperature ($\mu*$= 0.1). Instability of the solution at T = 10 K.

Table S3. Parameters of superconducting state of $Fm\bar{3}m$-$ThH_{10}$ at 100-300 GPa. Here $\gamma$ is Sommerfeld constant, $\mu^*$ is 0.1 (0.15). All calculations were done within Eliashberg formalism.

| *Parameter* | $Fm\bar{3}m$-$ThH_{10}$ | | |
|---|---|---|---|
| | *100 GPa* | *200 GPa* | *300 GPa* |
| $\lambda$ | 2.50 | 1.35 | 1.11 |
| $\omega_{log}$, *K* | 1073.1 | 1627.1 | 1775.3 |
| $T_C$, K | 241 (220) | 225 (197) | 201 (174) |
| $\Delta(0)$, meV | 52 (47) | 42 (36) | 38 (32) |
| $H_C(0)$, T | 71 (65) | 51 (44) | 39 (33) |
| $\gamma$, mJ/mol·K$^2$ | 11 | 6.4 | 5.2 |

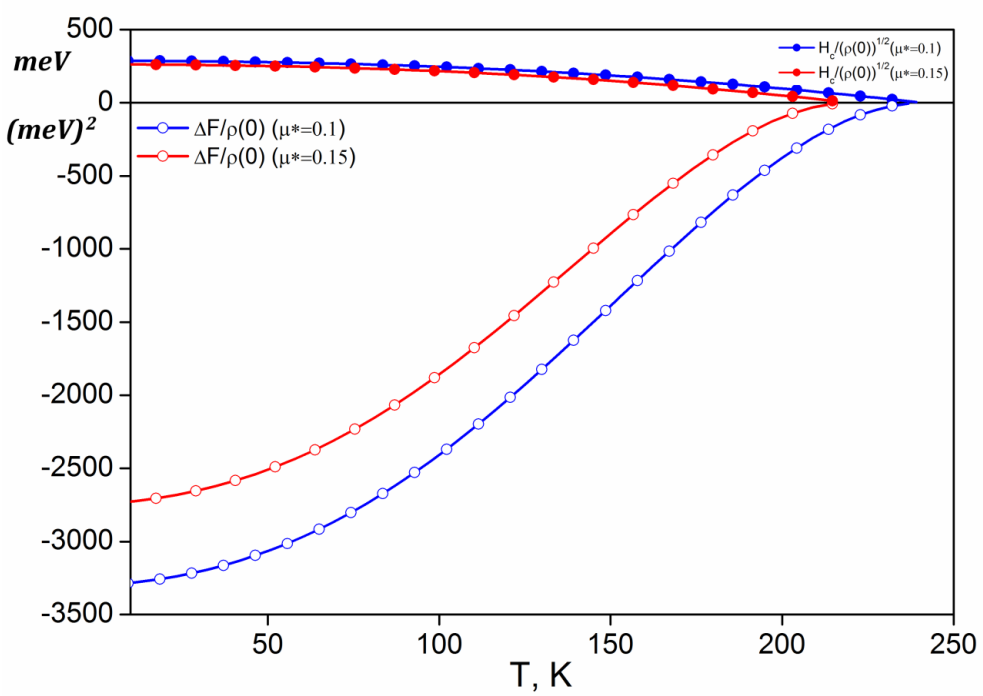


Fig. S8. Upper panel: the dependence of the thermodynamic critical field in $Fm\bar{3}m$-$ThH_{10}$ at 100 GPa on the temperature. Lower panel: the free energy difference between the superconducting state and the normal state as a function of the temperature. The negative values of ΔF prove the thermodynamic stability of the superconducting state. For the lowest temperature, that was taken into account, the free energy difference equals 3281.35 $meV^2$ and 2724.56 $meV^2$ for μ* = 0.1 and μ* = 0.15 respectively.

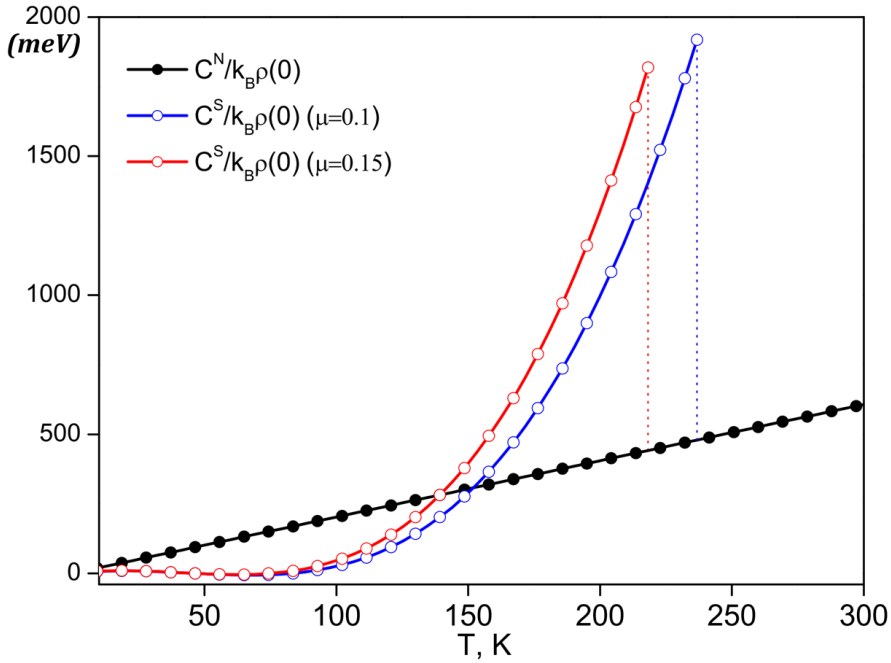


Fig. S9. The specific heat of the superconducting state ($C_S$) and the normal state ($C_N$) as a function of the temperature in $Fm\bar{3}m$-$ThH_{10}$ at 100 GPa.

## Electronic properties of Th-H phases

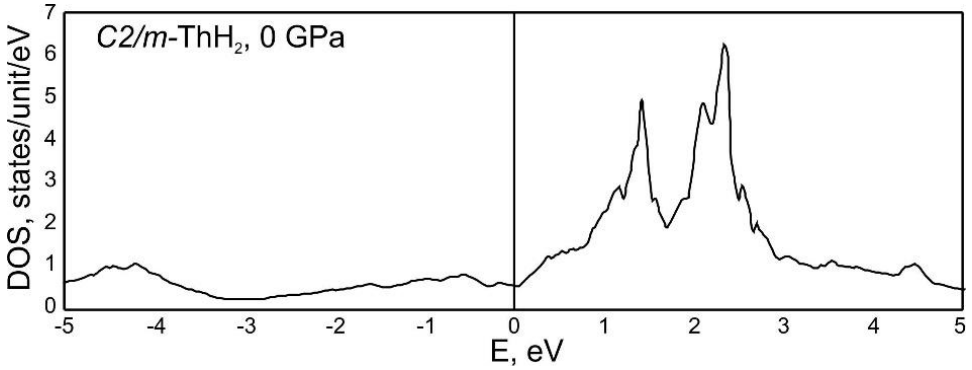


Fig. S10. Electronic density of states of *C2/m*-$ThH_2$ at 0 GPa. DOS($E_F$) = 0.35 states/unit/eV

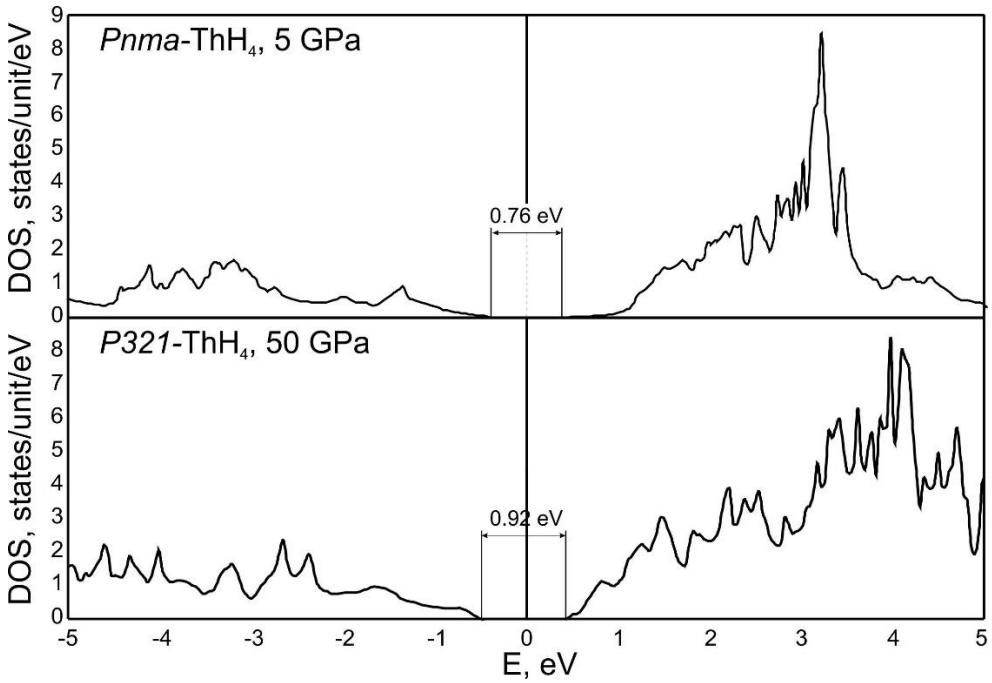


Fig. S11. Electronic densities of states of *Pnma*-$ThH_4$ and *P321*-$ThH_4$ at 5 and 50 GPa, respectively.

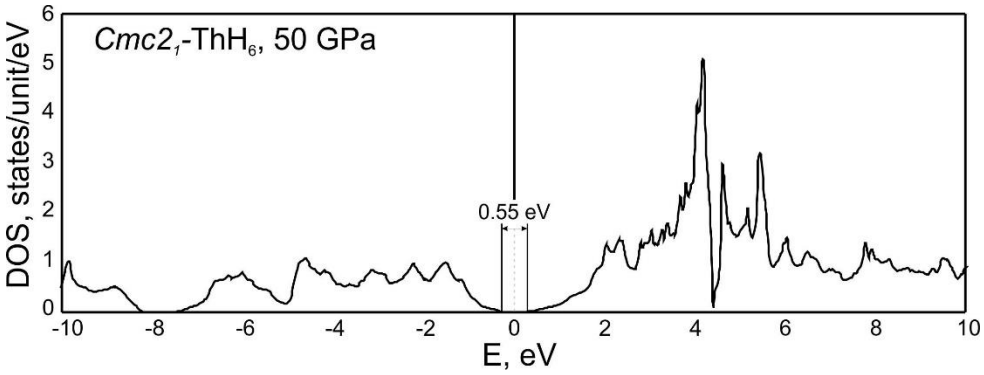


Fig. S12. Electronic density of states of *Cmc2₁*-$ThH_6$ at 50 GPa.

## Eliashberg spectral functions for $ThH_3$, $Th_3H_{10}$ and $ThH_7$ phases

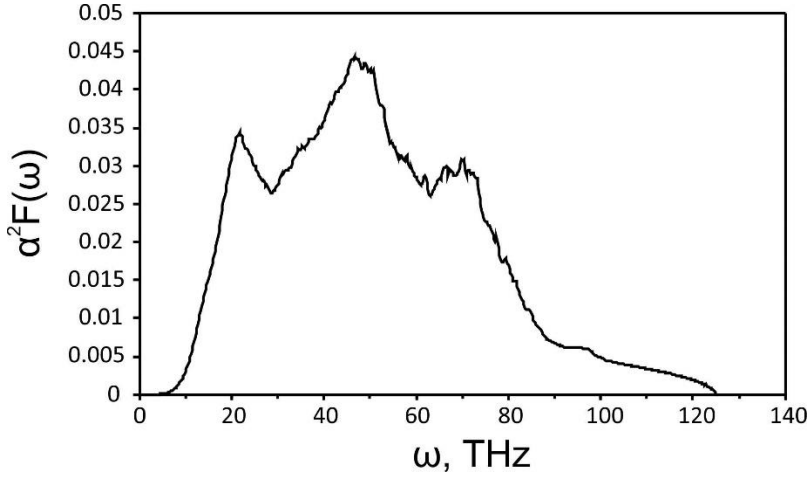


Fig. S13. Eliashberg function $\alpha^2F(\omega)$ of $R\bar{3}m$-$ThH_3$ at 100 GPa

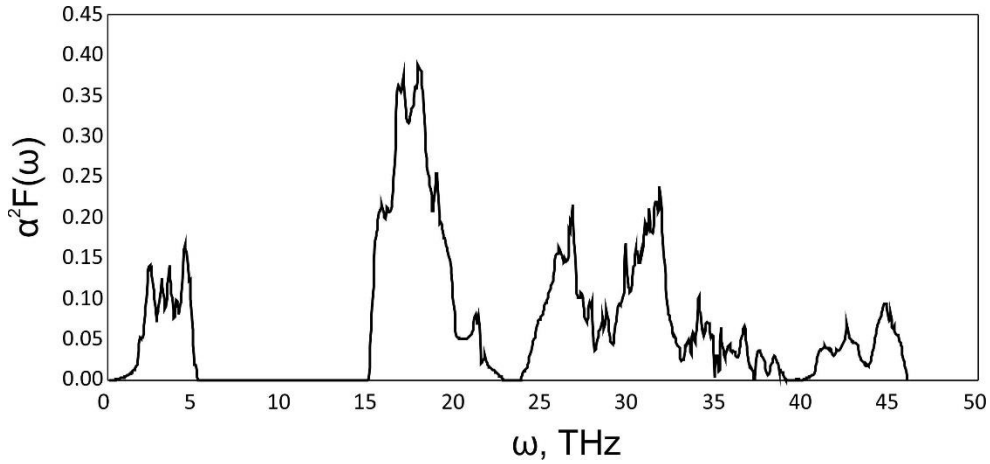


Fig. S14. Eliashberg function $\alpha^2F(\omega)$ of $Immm$-$Th_3H_{10}$ at 10 GPa

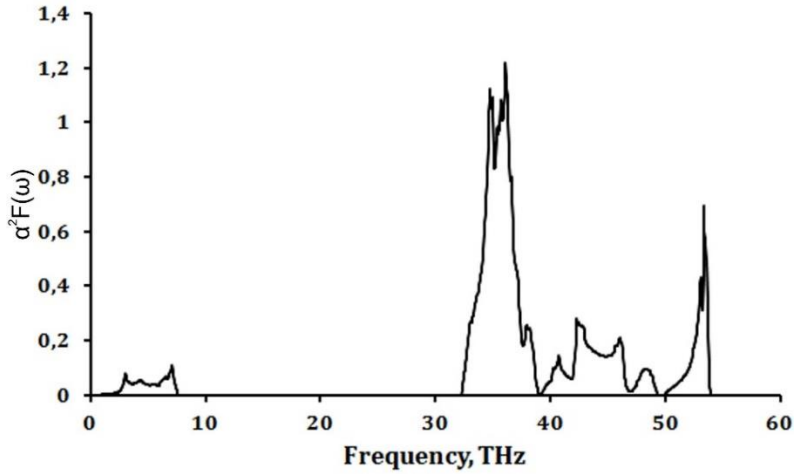


Fig. S15. Eliashberg function $\alpha^2F(\omega)$ of $I4/mmm$-$ThH_4$ at 85 GPa

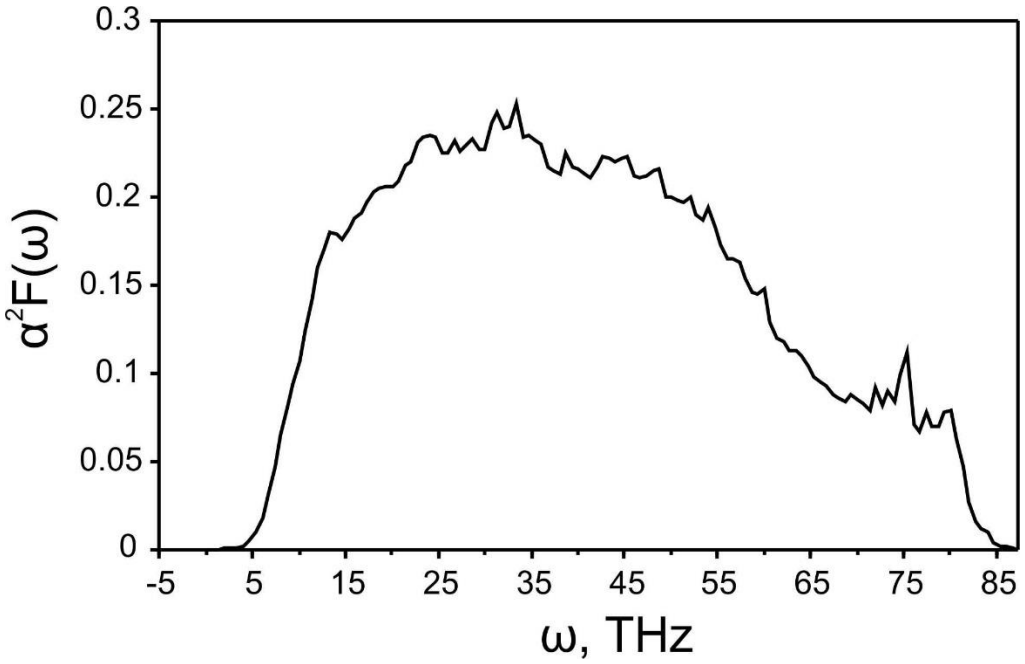


Fig. S16. Eliashberg function $\alpha^2F(\omega)$ of $P2_1/c$-$ThH_7$ at 100 GPa

**Dependence of $T_C$ on the pressure for $ThH_{10}$**

Here we describe a detailed analysis of pressure dependence of $T_C$ of $ThH_{10}$ phase. Fig. S14 shows the electronic DOS of $ThH_{10}$ calculated at 100, 200 and 300 GPa. All the data for analysis are summarized in Table S4. It is clearly seen from both Table S4 and Fig. S14 that the density of states at Fermi level decreases linearly with pressure for $ThH_{10}$.

Table S4. Calculated data for in $Fm\bar{3}m$-$ThH_{10}$ supercell.

| **$ThH_{10}$** | | | | | | |
|---|---|---|---|---|---|---|
| *P, GPa* | *Cell volume, $A^3$* | *$N_f$, states/unit/eV* | *$\omega_{log}$ ,K* | *$\lambda$* | *$T_C$ (A-D)*, K* | *$ln[T_C/\omega_{log}]$* |
| 100 | 248.8 | 0.61 | 1073.1 | 2.50 | 221.1 | -1.579 |
| 200 | 205.4 | 0.53 | 1627.1 | 1.35 | 182.6 | -2.187 |
| 300 | 183.2 | 0.48 | 1775.3 | 1.11 | 155.4 | -2.436 |

*Full Allen-Dynes (eq. (1))

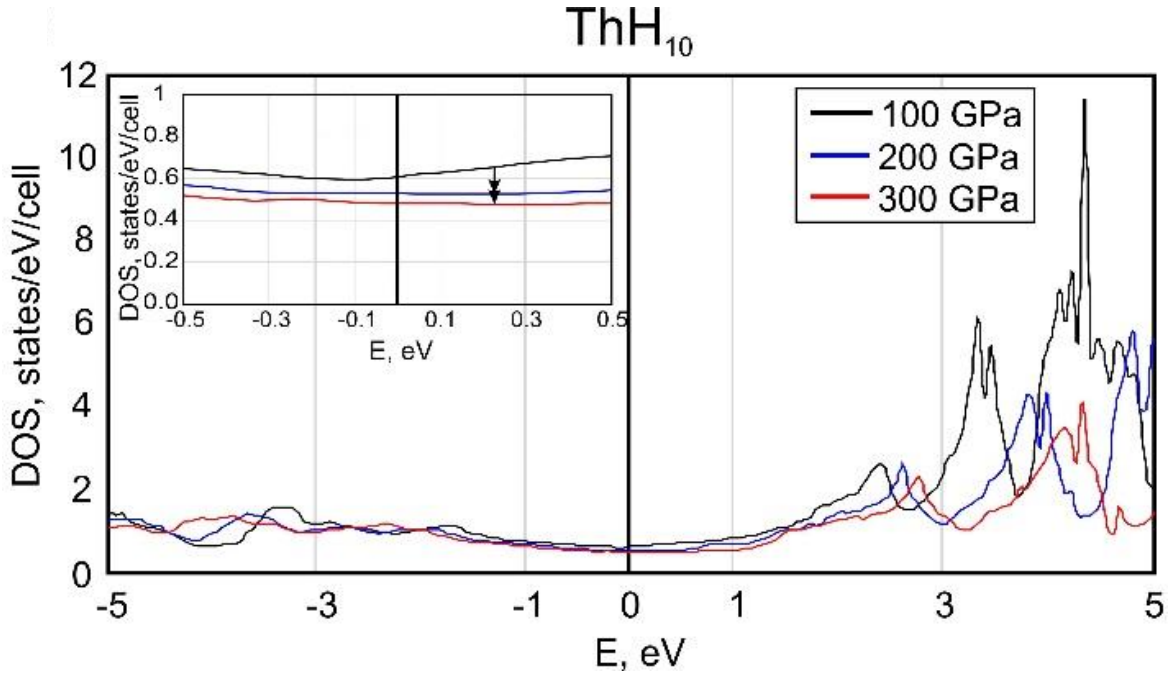


Fig. S17. Electronic densities of states of $ThH_{10}$ as a function of pressure. Fermi level is set to zero. Inset shows zoomed region from -0.5 to 0.5 eV for better view of DOS at Fermi level.

Results for $ThH_{10}$ show linear dependence of logarithmic frequency on pressure which can be well described by the following formula:

$$\gamma = \left(\frac{\partial\, ln(\omega)}{\partial\, ln(V)}\right)_T, \tag{S6}$$

where γ is the Grüneisen parameter, showing only small dependence on pressure and for most materials equal to ~1-1.5.

Calculated gradient of the critical temperature dependence $dT_C/dP$ for $ThH_{10}$ phase is negative as for the majority of metals and equals to $-3.85 \cdot 10^{-5}$ K/atm at 100 GPa. This value is similar to values for low-$T_C$ superconducting metals like Hg, Ga, Bi-II[20]. This value is also similar to that of $CaH_6$ phase from Ref.[21] where the $dT_C/dP = -3.34 \cdot 10^{-5}$ K/atm. Similarity of pressure dependence of $T_C$ for $ThH_{10}$ with other metals opens a new way of using the well-known empirical equation for low-$T_C$ superconductors:

$$-ln\left(\frac{T_C}{\omega_{log}}\right) = Cv^{-\varphi}, C > 0 \tag{S7}$$

with constant $C$ and $\varphi$ calculated earlier for non-transition metals ($\varphi = 2.5 \pm 0.6$)[22,23]. From calculated data (interpolation of $ln[T_c/\omega_{log}]$ function by $a \times v^b$ law) we can directly determine the coefficients $\varphi = 1.446$, $C = 4650.1$ ($R^2 = 0.98$), see Table S4.

Using the modified McMillan equation (see eq. (2)) we derived the dependence of the EPC coefficient on the pressure as:

$$T_C = \frac{\omega_{log}}{1.2} exp\left(\frac{-1.04(1+\lambda)}{\lambda - \mu^* - 0.62\lambda\mu^*}\right)$$
$$ln\left(\frac{T_C}{\omega_{log}}\right) = ln\left(\frac{1}{1.2}\right) + \left(\frac{-1.04(1+\lambda)}{\lambda - \mu^* - 0.62\lambda\mu^*}\right)\Big|_{\mu^*=0.1} \rightarrow 0.1823 + \frac{1.04(1+\lambda)}{0.938\lambda - 0.1} = Cv^{-\varphi} \quad \text{(S8)}$$

As a result, we obtained the following equation:

$$\lambda(P) = 0.1066 \times \frac{Cv^{-\varphi} + 10.22}{Cv^{-\varphi} - 1.291} \quad \text{(S9)}$$

For better comparison we summarized the obtained data in the Table S5 and show it in Fig. S14.

Table S5. Comparison of numerical and analytical results for $ThH_{10}$

| *P, GPa* | *$T_C$ (A-D), K* | *$T_C$ (eq. (S7)), K* | *λ (QE)* | *λ (eq. (S9)) ($\mu^*$ = 0.1, φ(McM) = 1.35)** |
|---|---|---|---|---|
| 100 | 221.1 | 219.4 | 2.50 | 2.29 |
| 200 | 182.6 | 187.9 | 1.35 | 1.47 |
| 300 | 155.4 | 141.2 | 1.11 | 1.03 |

*$\varphi$(McM) – is φ based on modified McMillan equation for $T_C$.

## References


(1) Eliashberg, G. M. Interactions between Electrons and Lattice Vibrations in a Superconductor. *JETP* **1959**, *11* (3), 696–702.

(2) Szczęśniak, R. The Numerical Solution of the Imaginary-Axis Eliashberg Equations. *Acta Phys. Pol. A* **2006**, *109* (2), 179–186.

(3) Szczęśniak, R. The Selected Thermodynamic Properties of the Strong-Coupled Superconductors in the van Hove Scenario. *Solid State Commun.* **2006**, *138* (7), 347–352.

(4) Durajski, A. P.; Szczęśniak, D.; Szczęśniak, R. Study of the Superconducting Phase in Silicene under Biaxial Tensile Strain. *Solid State Commun.* **2014**, *200*, 17–21.

(5) Beach, K. S. D.; Gooding, R. J.; Marsiglio, F. Reliable Padé Analytical Continuation Method Based on a High-Accuracy Symbolic Computation Algorithm. *Phys. Rev. B* **2000**, *61* (8), 5147–5157.

(6) Bardeen, J.; Cooper, L. N.; Schrieffer, J. R. Theory of Superconductivity. *Phys. Rev.* **1957**, *108* (5), 1175–1204.

(7) Carbotte, J. P. Properties of Boson-Exchange Superconductors. *Rev. Mod. Phys.* **1990**, *62* (4), 1027–1157.

(8) Liu, H.; Naumov, I. I.; Hoffmann, R.; Ashcroft, N. W.; Hemley, R. J. Potential High-$T_C$ Superconducting Lanthanum and Yttrium Hydrides at High Pressure. *Proc. Natl. Acad. Sci.* **2017**, *114*, 6990–6995.

(9) Durajski, A. P.; Szczęśniak, R.; Pietronero, L. High-Temperature Study of Superconducting Hydrogen and Deuterium Sulfide. *Ann. Phys.* **2016**, *528* (5), 358–364.

(10) Jarosik, M. W.; Drzazga, E. A.; Domagalska, I. A.; Szczęśniak, K. M.; Stępień, U. Description of the Thermodynamic Properties of $BiH_5$ and $BiH_6$ Superconductors beyond the Mean-Field Approximation. *Solid State Commun.* **2018**, *279*, 27–29.

(11) Durajski, A. P. Quantitative Analysis of Nonadiabatic Effects in Dense $H_3S$ and $PH_3$ Superconductors. *Sci. Rep.* **2016**, *6*, 38570.

(12) Jarosik, M. W.; Szczęśniak, R.; Wrona, I. A.; Kostrzewa, M. Non-BCS Superconducting State in Yttrium Hydride at a Record Low Value of the External Pressure. *Solid State Commun.* **2017**, *250*, 5–8.

(13) Flores-Livas, J.; Sanna, A.; Gross, E. K. U. High Temperature Superconductivity in Sulfur and Selenium Hydrides at High Pressure. *Eur. Phys. J. B* **2016**, *89* (3), 63.

(14) Szczęśniak, R.; Durajski, A. P. Superconductivity Well above Room Temperature in Compressed $MgH_6$. *Front. Phys.* **2016**, *11* (6), 117406.

(15) Nakayama, K.; Sato, T.; Terashima, K.; Arakane, T.; Takahashi, T.; Kubota, M.; Ono, K.; Nishizaki, T.; Takahashi, Y.; Kobayashi, N. Doping Dependence of the Gap Anisotropy of the High-Temperature $YBa_2Cu_3O_{7-\delta}$ Superconductor. *Phys. Rev. B* **2009**, *79* (14), 140503.

(16) Nishiyama, M.; Kinoda, G.; Shibata, S.; Hasegawa, T.; Koshizuka, N.; Murakami, M. Low Temperature Scanning Tunneling Spectroscopy Studies of High $J_C$ $NdBa_2Cu_3O_{7-\delta}$ Single Crystals. *J. Supercond. Nov. Magn.* **2002**, *15* (5), 351–354.

(17) Kugler, M.; Levy de Castro, G.; Giannini, E.; Piriou, A.; Manuel, A. A.; Hess, C.; Fischer, Ø. Scanning Tunneling Spectroscopy on $Bi_2Sr_2Ca_2Cu_3O_{10+\delta}$ Single Crystals. *J. Phys. Chem. Solids* **2006**, *67* (1), 353–356.

(18) Kondo, T.; Santander-Syro, A. F.; Copie, O.; Liu, C.; Tillman, M. E.; Mun, E. D.; Schmalian, J.; Bud'ko, S. L.; Tanatar, M. A.; Canfield, P. C.; et al. Momentum Dependence of the Superconducting Gap in $NdFeAsO_{0.9}F_{0.1}$ Single Crystals Measured by Angle Resolved Photoemission Spectroscopy. *Phys. Rev. Lett.* **2008**, *101* (14), 147003.

(19) Ding, H.; Richard, P.; Nakayama, K.; Sugawara, K.; Arakane, T.; Sekiba, Y.; Takayama, A.; Souma, S.; Sato, T.; T. Takahashi; et al. Observation of Fermi-Surface–Dependent Nodeless Superconducting Gaps in $Ba_{0.6}K_{0.4}Fe_2As_2$. *EPL Europhys. Lett.* **2008**, *83* (4), 47001.
(20) Brandt, N. B.; Ginzburg, N. I. Superconductivity at High Pressures. *Sov. Phys. Uspekhi* **1969**, *12* (3), 344.
(21) Wang, H.; Tse, J. S.; Tanaka, K.; Iitaka, T.; Ma, Y. Superconductive Sodalite-like Clathrate Calcium Hydride at High Pressures. *Proc. Natl. Acad. Sci.* **2012**, *109* (17), 6463–6466.
(22) Rohrer, H. Druck- und Volumeneffekte in der Supraleitung. *Helv Phys Acta* **1960**, *33*, 675–705.
(23) Olsen, J. L.; Rohrer, H. The volume dependence of the electron level density and the critical temperature in superconductors. *Helv Phys Acta* **1960**, *33*, 872–880.